Sediment Corrections for Distributed Acoustic Sensing

Alister Trabattoni[1], Clara Vernet[1], Martijn van den Ende[1], Marie Baillet[1], Bertrand Potin[1,2], Diane Rivet[1]

[1] *Université Côte d'Azur, Observatoire de la Côte d'Azur, CNRS, IRD, Géoazur, France* (alister.trabattoni@gmail.com)
[2] *Departamento de Geofísica, University of Chile, Santiago, Chile*

Abstract

On continental margins, sediments cause significant and spatially variable delays in seismic phase arrival times. The strong impedance contrast of the sediment-bedrock interface causes P-wave splitting that is clearly seen on Distributed Acoustic Sensing recordings of earthquakes, resulting in additional phase arrivals that must be picked separately. We introduce *sediment corrections* to correctly account for those additional phases in the hypocenter localization procedure.

Conceptually, the sediment correction method differs from the commonly-used *station corrections;* instead of introducing a mathematically optimal constant time delay for each station and each phase, the corrections are derived from a physical, first-order modeling of the wave propagation in the sediments. To calibrate the sediment corrections, a two-step procedure is adopted: (i) the delay between the P-phase and the converted Ps-phase is taken as a proxy of the sediment thickness; (ii) the P- and S-wave speeds are determined through inversion.

We show that sediment corrections are able to account for most of the observed bias while considerably reducing the number of free parameters compared to classical station correction. Moreover, the observed local delays are almost fully explained by the presence of the sedimentary layer, rather than by the 3D velocity variations of the bedrock. We retrieve v_P and v_S values that are compatible with values commonly found for sediments. Given the simplicity and physical foundation of the proposed method, we recommend the use of sediment corrections over station corrections whenever significant P-wave splitting can be observed.

Key Points

- We propose a novel inversion method to account for the presence of shallow sedimentary layers in hypocenter localization
- The inferred sediment properties explain the travel time discrepancies compared to the regional velocity model
- The sediment correction method improves hypocenter localization efforts with a small number of free parameters

Plain Language Summary

Loose sediments on the ocean floor strongly affect how seismic waves travel from the earthquake hypocenter to the surface. The most important effect is that sediments slow down the seismic waves, causing them to arrive later at the seismic instruments. These delays can make it difficult to accurately locate the source of earthquakes.

This study proposes a new method called *sediment corrections*. We used the Distributed Acoustic Sensing technology to track delays caused by sediment along a telecommunication cable offshore central Chile, located in a very active subduction zone. Using a simple physical model of how seismic waves travel through

sediments, we recovered the main structural features of the sediments beneath the cable. Using the properties of the sediments, we then improved the localization of the earthquake sources. Importantly, this method has the potential to be applied in different sedimentary environments, reducing the challenges associated with interpreting data collected in such geological areas.

1. Introduction

Distributed Acoustic Sensing (DAS) is rapidly becoming a standard approach for geophysical data acquisition. The incredible spatial density of DAS recordings permits an unprecedented view of the seismic wavefield. The dimensionality of the data (evenly sampled in space and time) greatly increases the interpretability of seismic phase arrivals, as they can be visually tracked in space and time. Furthermore, the robustness and flexibility of fiber-optic cables unlocks the possibility of deploying large and dense arrays in harsh or hard to access locations, such as volcanoes or the deep ocean. Along with those improvements comes the burden of new technical and scientific challenges. Typically, DAS data is stored in the form of the strain rate component along the cable direction. As previous studies have shown, this implies an increased response to local site effects and to locally scattered waves especially in soft sedimentary areas (van den Ende & Ampuero, 2021; Trabattoni et al., 2022).

Another aspect of consideration that is specific to DAS, is the intricacies of the seismic wavefield. Owing to the spatially uniform discretization of a DAS measurement, strong wavefront deformation can be readily observed in most sedimentary areas. In the context of a small (one kilometer) on-land deployment, Trabattoni et al. (2022) found that direct body waves were not observable. Scattered and converted phases dominated the wavefield, resulting in waveform patterns that were primarily influenced by the sedimentary basin rather than by the seismic source. This prevented the use of any classical localization approach such as travel time inversion or beamforming. In the context of an offshore deployment in Central Chile, Trabattoni et al. (2023) observed similar seismic wave content dominated by locally refracted and reverberated surface waves. Because of the appreciable length of the sensed fiber-optic cable (150 km), the long-range moveout of the body wave arrivals could still be estimated. By converting the strain rate data into particle displacement through spatio-temporal integration, the amplitude of slow scattered waves was greatly attenuated. As a result, faint but highly spatially coherent direct body-wave arrivals could be discerned right before less coherent but higher amplitude phase arrivals. The consistent observation of these multiple arrivals was interpreted as the signature of phase splitting at the bedrock/sediments interface.

These observations raise the question of how one should address local site effects that are so prominent in the DAS data which presents two distinct challenges: (i) Sediments split the usual P- and S-wave arrivals into several observable arrivals which must be identified accordingly. (ii) Regional velocities models can only account for the arrival of direct P- and S-waves, one must find a way to incorporate the sedimentary effects for accurate localization of seismic events.

A possible solution is to use *station corrections*. The objective of this framework is to determine a constant time delay for each receiver and for each phase. This time delay acts as a bias term to capture sedimentary delays, and permits a different modeled travel time for the transmitted and converted phase. While this approach has proven effective in reducing phase arrival residuals, it requires one to invert for a large number of parameters and can potentially be subject to overfitting.

To address the challenges of station corrections, and to account for the wavefront deformation produced by the sediments, we introduce a simple yet effective solution called *sediment corrections*. This method is based on a physical modeling of the sediments and only requires to invert for two parameters (the P- and S-wave speed of the sediments). We focus on the case of an offshore deployment in Central Chile, and we first

present a number of observations of phase splitting and wavefield distortion. Then, a first-order modeling of the wave propagation in the sediment will be introduced, which forms the basis of our proposed method. Finally, we detail the sediment corrections method and compare its performance with that of the station corrections method.

2. Data

To illustrate the proposed approach, we analyze DAS strain rate recordings from a pilot experiment conducted in 2021 in Central Chile. An OptoDAS interrogator (Alcatel Submarine Networks) was connected to an offshore dark telecom fiber-optic cable that connects Concón to La Serena and belongs to the GTD (Gente Totalmente Dispuesta) telecom network (Fig. 1). The data were acquired at 500 Hz and subsequently down sampled to 125 Hz. The effective gauge length was set to 8.16 m with a corresponding channel spacing of 4.08 m. The experiment took place from October 27th to December 3rd of 2021, recording continuously during this interval. In this study we focused on a 100-km section that starts at a distance of 20 km from the interrogator up to 120 km (Fig 1a). This region of interest was bounded by strong ocean gravity waves dominating the data near the coast, and by the reduced optical budget (poor signal-to-noise ratio) after a distance of 120 km. On this section, the depth of the cable ranges from a few hundred meters to around 2 km below sea level. Notably, this cable is located between the coast and the Chilean subduction trench, bordering the regions of destructive historical earthquakes such as the 2015 M_w 8.3 Illapel earthquake.
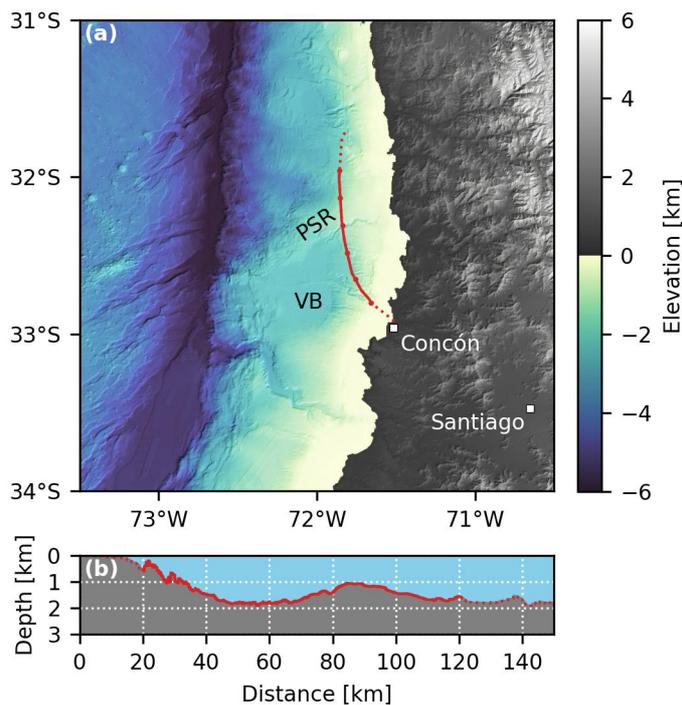
Figure 1. Central Chile offshore DAS deployment. (a) Location of the first 150 km of the fiber-optic cable that links Concón to La Serena. (b) Depth of the cable as a function of the distance from the interrogator. The cable (red line, marked every 20 km) crosses several underwater canyons (major ones at 20, 30 and 80 km). It passes through the Valparaiso forearc basin (VB) surroundings, and overlays the Punta Salina Ridge (PSR – from 80 to 100 km). Because of signal quality considerations, we focus on the range from 20 to 120 km from the interrogator (dotted line is unused).

Through automated detection and manual inspection of the one-month long dataset, thousands of earthquakes have been identified. On most earthquakes, distinct P-wave and S-wave trains can be observed. By converting the natively recorded strain rate to displacement through spatio-temporal integration, mean removal of a 1 km sliding window (Trabattoni et al., 2023), 2 Hz high pass filter, and further inspection, we observed that ~5-10% of the events display three discrete arrivals (Fig 2a.). A faint first and highly spatially

coherent arrival is closely followed by a much more distorted wavefront (Fig 2b). Later, a third arrival that is as similarly distorted as the second one emerges. As proposed by Trabattoni et al. (2023) the first arrival is interpreted as the direct P-wave arrival, the second arrival is interpreted as the conversion of the P-wave into an S-wave at the bedrock/sediment interface, and the third arrival is interpreted as the direct S-wave arrival. In this work, we refer to those three phases as Pp, Ps and Ss, respectively, while the notation of P and S will be reserved for the theoretical arrivals given by the regional model in a case of sediments being absent. It is interesting to note that Sp (S-wave converted to P-wave) was never clearly observed, likely due to the amplitude of that phase being smaller than the reverberation and scattering of the P wave train, effectively obscuring it.
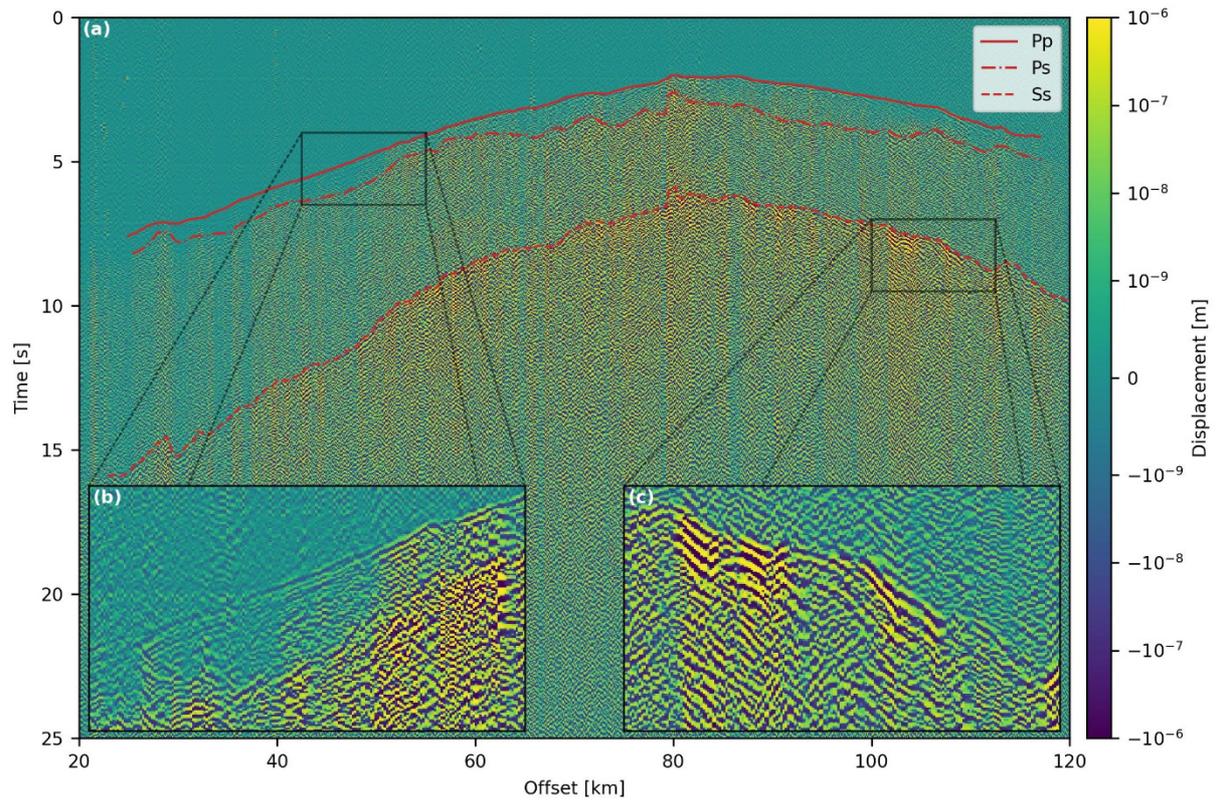
Figure 2. Observation and picking of the splitting of the P-wave phase into Pp and Ps along with the transmitted S-wave into the Ss phase. (a) Recovered displacement waveforms for a small regional earthquake that occurred a few tens of kilometers away from the cable. Three arrivals can be observed (Pp, Ps, and Ss). For most events the Pp cannot be observed. (b) The Pp arrival has smaller amplitude but more regular wavefront than the Ps arrival. (c) While having a moveout that is overall different from that of the Ps phase, the Ss arrival has similar wavefront structure as the Ps.

We selected 30 high-quality earthquakes with clear Pp arrival and manually picked the Pp, Ps and Ss arrivals. We developed a software that allowed us to draw continuous phase fronts onto the 2D distance-time representation and easily adjust the contrast and range of the colormap (see Open Research). The freely drawn phase front were then linearly interpolated on the positions of the channels of interest. This allowed each operator to process several earthquakes per hour despite the high number of channels (close to 25,000). The Pp arrival, while being the faintest, was relatively easy to pick owing to its high spatial coherency and temporal isolation from reverberations (Fig 2b). The Ps arrival was more challenging to distinguish, and horizon selection was sometimes difficult because of the reverberations of the Pp arrival (Fig 2b). We adopted a conservative strategy, picking only sections of the cable with a clear onset (rather than visually interpolating). Owing to its large amplitude, the Ss phase was usually quite unambiguous to pick (Fig 2c). We empirically estimated the uncertainties to be 0.1 s for the Pp arrival and 0.3 s for the Ps an Ss arrival.

3. Methods & Results

To achieve a correct earthquake hypocenter localization using the three identified phases, we adopt the framework of *station corrections*. The deviation of the time of arrivals from theoretical arrivals in the absence of sediments is modeled as a constant delay for each DAS channel and phase. We first propose a first-order modeling of the sediments and confirm the validity of assuming constant delays by measuring and analyzing the Pp to Ps lag for a number of events. We then apply station corrections and note that the corrections for the three phases are highly correlated. Finally, we propose *sediment corrections* which models the corrections in term of the sediment thickness and wave speeds, reducing the number of unconstrained parameters and proving that sediments are indeed responsible of most of the local effects.

3.1. Sediment modeling

We propose a simple modeling of the sediments, as schematically summarized in Fig. 3. The model consists of replacing part of the solid earth below the cable by a distinct sedimentary layer with corresponding reduced P- and S-wave velocities. Sediments are known to have significant velocity gradients but overall, the propagation time along the entire layer can be approximated using layer-averaged equivalent velocities that are chosen to give the correct travel time for a vertical ray. In this work, we assume that those average equivalent velocities are spatially uniform.
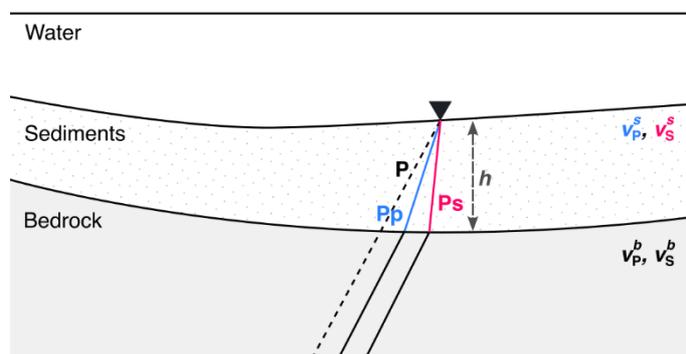
Figure 3. Modeling of the wave ray paths in the sediments for an incoming P-wave (the same pattern applies for the S-wave). In the absence of sediments, a receiver (black inverted triangle) would measure a time of arrival t_P that can be accurately modeled using regional velocity models. Because of the sediments, this hypothetical arrival is split and delayed resulting in two measured arrival times (t_{Pp} and t_{Ps}) that represent the transmitted and converted waves at the bedrock/sediments interface.

Furthermore, we assume almost vertical ray propagation through the sediment layer, which is justified by the high velocity contrast at the interface that is assumed to be flat (e.g., Doran & Laske, 2019). We implicitly suppose that the bathymetry and the sediment thickness variations are smoothly varying in space, otherwise 3D effects should be considered (which may be relevant for rugged terrains like an underwater canyon). Under this assumption, the ray path length can be accurately approximated by h, the sediment thickness. In keeping with the first order nature of the modeling, we also consider that the path length of the theoretical ray P in case of absence of sediments, once it has entered the sediment layer, is approximated by h. This part of the ray path is implicitly modeled when computing travel time from regional models. The velocities v_P^b and v_S^b of the bedrock are taken from the 1D velocity model used for the hypocenter localization and are then supposed to be known quantities of the problem. The velocities v_P^s and v_S^s in the sediments need to be determined. Using those simplifications, the arrival times t_{Pp}, t_{Ps} and t_{Ss} can be expressed in terms of the theoretical times of arrival without sediments (τ_P and τ_S) as:

$$t_{Pp} = \tau_P + h \left(\frac{1}{v_P^s} - \frac{1}{v_P^b} \right) \tag{1}$$

$$t_{Ps} = \tau_P + h \left(\frac{1}{v_S^s} - \frac{1}{v_P^b} \right) \tag{2}$$

$$t_{Ss} = \tau_S + h \left(\frac{1}{v_S^s} - \frac{1}{v_S^b} \right) \tag{3}$$

Interestingly, the time delay Δt between Pp and Ps does not depend on the used regional propagation model.

$$\Delta t = t_{Ps} - t_{Pp} = h \left(\frac{1}{v_S^s} - \frac{1}{v_P^s} \right) \tag{4}$$

To validate the hypothesis of almost vertical ray propagation, we estimated the variability of Δt for the 30 manually picked events (Fig. 4). The standard deviation of the observed Δt, estimated per-channel and averaged over all the channels, was found to be 0.10 s, which is comparable with the measurement uncertainties. This suggests that the uncertainty introduced by our simplifying assumptions is less than the precision of the manual picking. The value of Δt can be used as a zeroth-order corrections (see later) and will be refered to as the *delay corrections*.
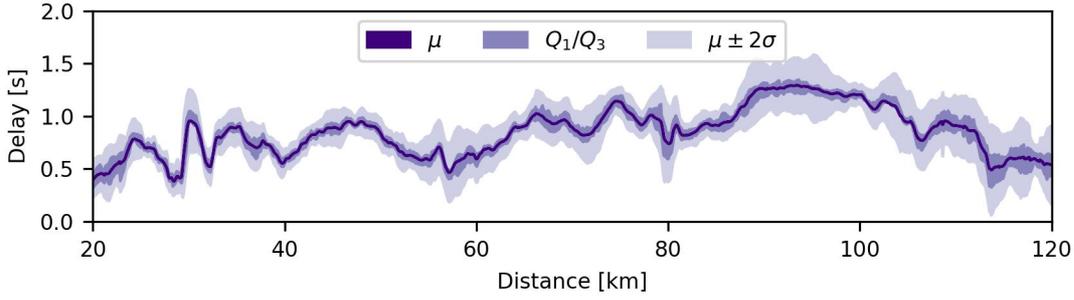
Figure 4. Time difference of arrival Δt between the Pp and the Ps phases for 30 manually picked events. The mean (μ), first and third quartiles (Q_1/Q_3) and an estimation of the 95% confidence interval using the per-channel standard deviation (σ) show that the Δt can be considered constant from one earthquake to another at a given receiver location. The fluctuations of Δt as a function of space give a first indication of the sediments thickness variations.

3.2. Station corrections

As a reference for our proposed sediment correction approach, we first adopt the conventional station correction approach (e.g., Douglas, 1967; Pujol, 2000; Richards-Dinger & Shearer, 2000). Consider a given set of n earthquakes with hypocenters $R = \{\boldsymbol{r}_1, \dots, \boldsymbol{r}_n\}$ and origin times $T = \{t_1, \dots, t_n\}$, along with a given set of m receivers and a set of p phases of interest. The observables consist in a set O of picked arrival times t_{ijk}^O measured for the event i at the receiver j and for the phase k. Note that not every receiver records every phase arrival for each event: we denote $|O|$ the cardinality of O, which is the total number of picks. A classical objective function (or loss) for the hypocenter localization of a unique event without local corrections is:

$$L_i(\boldsymbol{r}_i, t_i | O_i) = \frac{1}{|O_i|} \sum_{t_{ijk}^O \in O_i} \left[\frac{t_{ijk}^O - \left(t_i + \tau_{jk}(\boldsymbol{r}_i) \right)}{\sigma_k} \right]^2 \tag{5}$$

In this expression, the computed travel time between r_i and the receiver j for phase k is denoted by $\tau_{jk}(r_i)$. The observational uncertainty associated with t_{ijk}^O is denoted σ_k (which here only depends on the phase type). O_i denotes the subset of picks that correspond to the event i. To solve the localization problem, this objective function is minimized with respect to the seismic source parameters r_i and t_i.

To capture highly localized variations in τ, the station correction method introduces a set C of correction terms c_{jk} associated with receiver j and phase k. Those corrections are jointly inverted with the hypocenter locations of the n events:

$$L(R,T,C|O) = \frac{1}{|O|} \sum_{t_{ijk}^O \in O} \left[\frac{t_{ijk}^O - \left(t_i + \tau_{jk}(r_i) + c_{jk} \right)}{\sigma_k} \right]^2 \tag{6}$$

The partial minimization of the origin times T (with other parameters fixed) can be solve analytically. This reduces the number of dimensions to explore. The dependence of the loss with T was removed in all the following by using the analytic solutions of the origin times t_i:

$$t_i(r_i, c_{jk}) = \frac{1}{|O_i|} \sum_{t_{ijk}^O \in O_i} \left[\frac{t_{ijk}^O - \left(\tau_{jk}(r_i) + c_{jk} \right)}{\sigma_k} \right] \tag{7}$$

For the forward propagation model, we used the 1D velocity model proposed by Marot et al (2014). We precomputed a travel-time lookup table using the 2D Eikonal solver FTeik (Noble et al., 2014). The lookup table spanned a region up to 100 km from the DAS cable with a grid spacing of 1 km. To account for the spherical nature of the Earth, the Earth flattening transformation was used. We took $\sigma_{Pp} = 0.1$ s and $\sigma_{Ps} = \sigma_{Ss} = 0.3$ s (see before).

To solve the minimization problem, we used an alternating update approach, adapting the framework initially proposed by Frohlich (1979). At each iteration l, we first solved the localization problem for each earthquake (i.e., partial minimization of the locations), assuming constant station corrections. A brute-force grid search on the entire area covered by the lookup table was performed. Then we minimized the corrections that were given as the average residuals over all events at each channel and each phase:

$$R^{l+1} \leftarrow \arg\min_R L\left(R, C^l | O \right) \tag{8}$$

$$c_{jk}^{l+1} \leftarrow \frac{1}{|O_{jk}|} \sum_{t_{ijk}^O \in O_{jk}} \left[t_{ijk}^O - \left(t_i(r_i, c_{jk}) + \tau_{jk}(r_i^{l+1}) \right) \right] \tag{9}$$

Here we denote O_{jk} the subset of all picks corresponding to a given receiver j and phase k.

In this kind of minimization problem, the choice of the initial values plays an important role. A good initialization increases the chances of finding the global optimum and improves the rate of convergence. We propose as initial value to assume that the Pp arrival is very close to the computed theoretical P arrival without sediments (it undergoes negligeable delay and distortion). The Ps and Ss arrivals both undergo the same Δt delay (eq. 4), that is fixed as the averaged observed delay between the Pp and the Ps arrival:

$$c_{jk}^0 = \begin{cases} 0 & \text{if } k = \text{Pp} \\ \Delta t & \text{if } k \in [\text{Ps, Ss}] \end{cases} \tag{10}$$

Those initial values correspond to the *delay corrections*. The choice of those initial corrections as the best initial guess is justified by the observation that the Pp arrival looks smooth (the P-wave traversing the sediment layer does not seem to be strongly affected) while the Ps and Ss arrival are very distorted and share the same structure (both undergoes the same important slowdown due to the very low S-wave speed

characteristic of the sediments). This zeroth-order correction has the advantage of not requiring any inversion.

A few dozen iterations of eqs. (8) and (9) were sufficient to achieve convergence close to machine precision. The loss decreased from 1.75 without any correction to 0.74 with delay corrections down to 0.39 with station corrections. The Ps and Ss station corrections terms were very similar (Fig. 5a), suggesting that these phases undergo similar delays. The Pp correction terms were found to be small but also highly correlated with the Ps and Ss terms (Fig. 5b&c). This correlation between correction values of the different observed phases was already observed for conventional station corrections (Jeffreys & Singh, 1973) and shows that corrections are proportional to a hidden variable, here likely the sediment thickness as proposed in eqs. (1) to (3). This motivates a correction approach that is founded on a physical model for sedimentary effects, allowing us to improve the inversion without potentially overfitting on 3D bedrock velocity deviations from the adopted 1D velocity model.
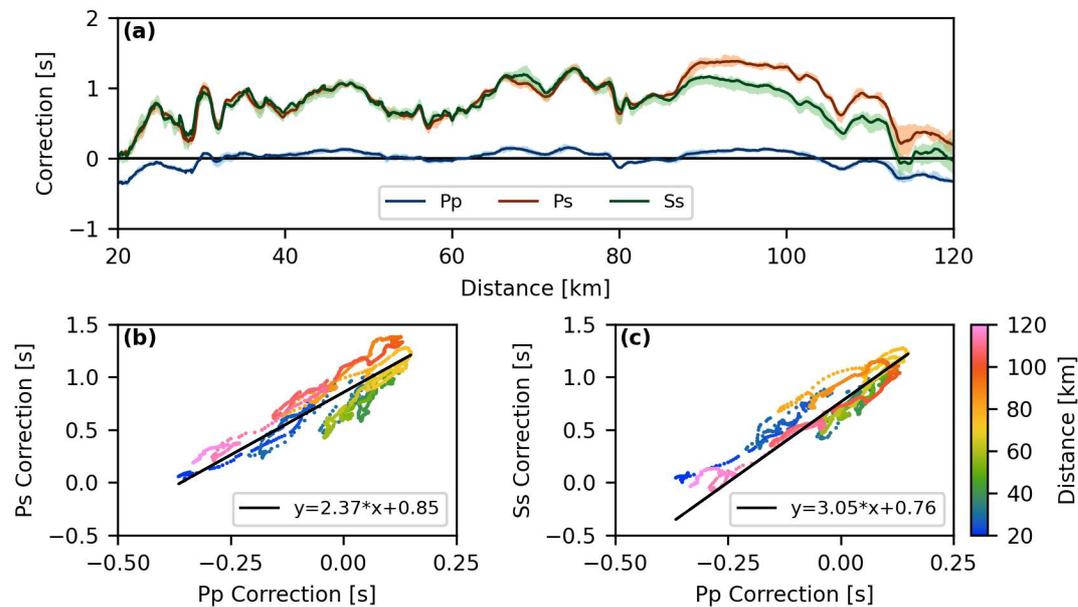
Figure 5. Station corrections. (a) Per channel and per phase. The Ps and Ss corrections look very similar, showing that those two phases undergo similar delays. The Pp correction looks as a lower-amplitude version of the Ps and Ss corrections. (b) Ps vs. Pp corrections and (c) Ss vs. Pp corrections. Pp corrections correlate very well with either Ps or Ss with a factor of about three.

3.3. Sediment corrections

Station corrections introduce a large number of parameters (one station correction per channel and per phase in addition to the earthquake source parameters) that must be inverted for, which increases the risk of overfitting, particularly for a small number of events. Here we introduce *sediment corrections* with the intent of using a simple physical modeling of seismic wave propagation in the sediments to reduce the number of unconstrained parameters and to gain valuable insight in the nature of the sediments. Sediment corrections also consider that local discrepancies from the computed theoretical arrival times can be modeled through constant per channel and per phase corrections. But in this approach, corrections are constrained by a simple physical modeling of the sediments (see before), effectively reducing the number of free parameters.

Rewriting eq. (4), it appears that the thickness of the sediments h_j at receiver j is proportional to Δt_j the average Pp to Ps time delay:

$$h_j = \frac{\Delta t_j}{\frac{1}{v_S^s} - \frac{1}{v_P^s}}$$ (11)

By substituting this equation into eqs. (1) to (3), the dependence of the correction term on the sediment layer thickness can be eliminated in favor of Δt_j at each jth channel (Δt_j being a measured quantities that we do not need to invert for):

$$c_{jk} = \begin{cases} \Delta t_j \dfrac{v_S^s}{v_P^b} \dfrac{v_P^b - v_P^s}{v_P^s - v_S^s} & \text{if } k = \text{Pp} \\[2ex] \Delta t_j \dfrac{v_P^s}{v_P^b} \dfrac{v_P^b - v_S^s}{v_P^s - v_S^s} & \text{if } k = \text{Ps} \\[2ex] \Delta t_j \dfrac{v_P^s}{v_S^b} \dfrac{v_S^b - v_S^s}{v_P^s - v_S^s} & \text{if } k = \text{Ss} \end{cases}$$ (12)

This reduces the number of correction related parameters to invert into eq. (6) to only two (v_P^s and v_S^s, with v_P^b and v_S^b being taken from the used regional velocity model). We proceed with a similar inversion procedure as described in the previous section by substituting eq. (11) into eq. (6). We alternate between optimization over the source parameters with constant v_P^s and v_S^s, and optimization over v_P^s and v_S^s with constant source parameters.

$$R^{l+1} \leftarrow \arg\min_{R} L\left(R, v_P^{s,l}, v_S^{s,l} \middle| O\right)$$ (13)

$$v_P^{s,l+1}, v_S^{s,l+1} \leftarrow \arg\min_{v_P^s, v_S^s} L\left(R^{l+1}, v_P^s, v_S^s \middle| O\right)$$ (14)

A few dozen iterations were necessary to converge near to machine precision. The partial minimization of eq. (14) was done with a generic global minimization algorithm (the Basin-Hopping implementation of SciPy – Wales & Doye, 1997).

At first glance, the resulting *sedimentary correction* terms look similar to the previous *station correction* terms (Fig. 6). Two main differences can be noted: (i) Sediment corrections are by definition always positive and provide an unbiased estimation of the origin time. In the station correction approach the origin time is mathematically unconstrained. A shift in the origin time can be compensated by the same shift of the corrections values. (ii) We get an estimate of the physical properties of the sediment layer that can be compared with those obtained using other imaging techniques.
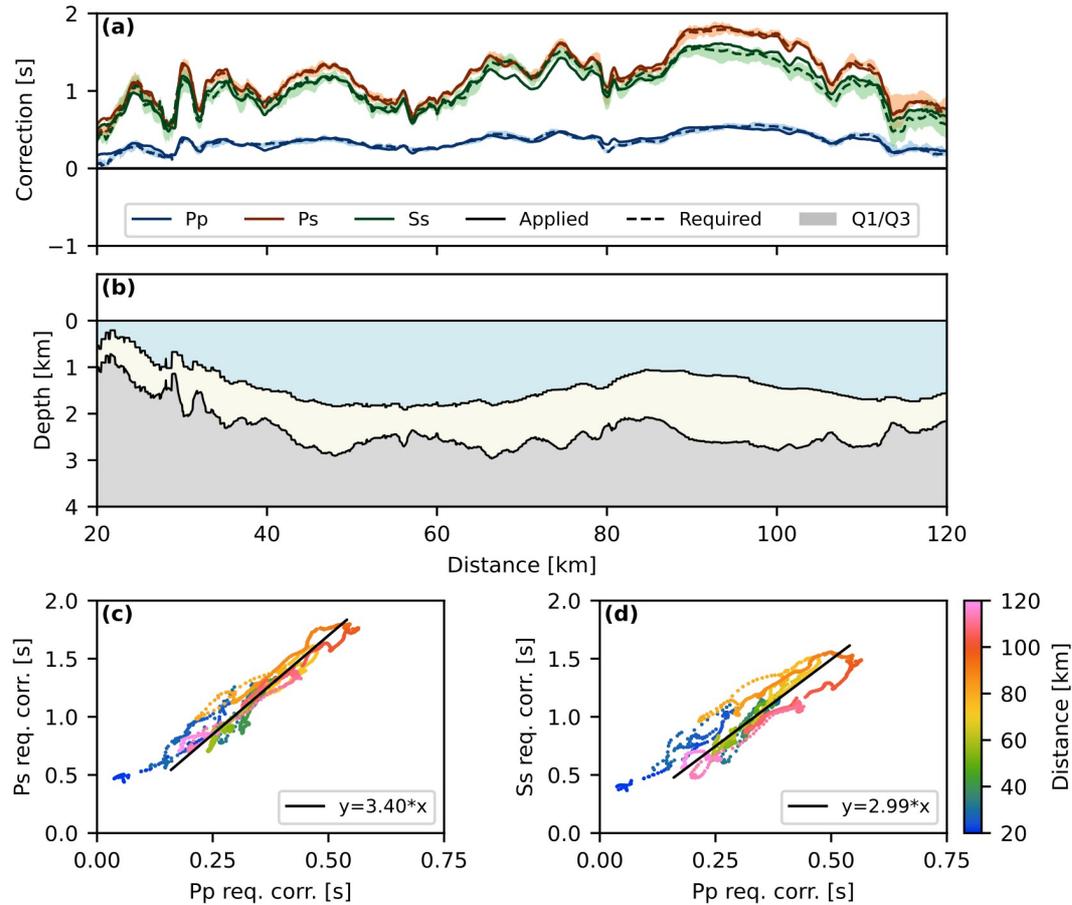
Figure 6. Sediment corrections. (a) Per channel and per phase applied (solid lines) and required (dashed lines) corrections. Required corrections are estimated as the average difference between modeled travel times without corrections and the observed times. The interquartile uncertainty is shown (Q1/Q3, filled areas). (b) Retrieved sediment thickness added bellow the local bathymetry along the cable (ocean in blue filled area, sediments in beige and bedrock in gray). (c) Ps vs. Pp and (d) Ss vs. Pp required corrections. Pp required corrections correlates very well with either Ps or Ss. Note that the same theoretical P arrival is used to estimate the Pp and Ps required corrections whereas the Ss ones are estimated with the theoretical S arrival. Inaccuracies in the estimated theoretical arrival times might explain the poorer correlation between Pp and Ss.

The *sediment corrections* inversion procedure converged toward velocities values of $v_P^s = 1.73$ km/s and $v_S^s = 0.68$ km/s, and a sediment thickness profile ranging from a few hundred meters to more than 1 km (Fig 6b). To evaluate the uncertainties, the conditional loss of v_P^s and v_S^s (i.e., by fixing the sources locations found at convergence) can be used (Fig. 7).
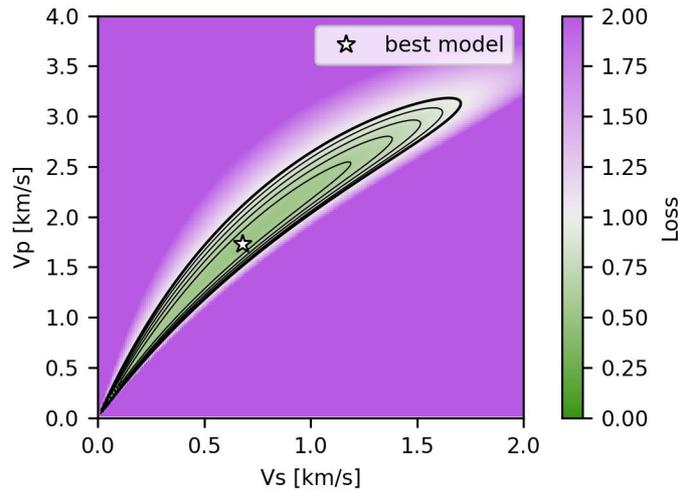
Figure 7. Partial loss as function of v_P^s and v_S^s at convergence. Contours are plotted in black every 0.1 step of loss from 1.0 (thicker line) down to 0.6. Note that values of v_P^s below 1.5 km/s (acoustic wave speed of water) are very unlikely, even in poorly consolidated sediments.

The values of v_P^s and v_S^s are strongly correlated, hence the inversion is mainly capable of constraining the v_P^s/v_S^s ratio. Running the inversion to convergence yields wave speed values that are anticipated for marine sediments (Hamilton, 1979): v_P^s is above the speed of sound in water and v_S^s is of the order of a few hundred meters per second. The retrieved sediment thicknesses compare with seismic reflection profiles made in the area (Contreras-Reyes et al., 2014; Contreras-Reyes et al., 2015). However, those regional studies suggest that sediment velocities should be slightly higher than our best model (e.g., $v_P^s > 2$ km/s). This is not inconsistent with the loss landscape that allows for a simultaneous increase of v_P^s and v_S^s. This would imply an increase in the estimation of the sediment thickness in Fig. 6a as this quantity is directly linked to the obtained velocities as a multiplicative term (eq. 11). This increase is also supported by the retrieved average ratio $v_P^s/v_S^s = 2.6$ which value is low and can only correspond to thick sediments (e.g., Zhu et al., 2020).

3.4. Localization improvements

One of the main motivations for applying correction terms is to reduce location bias in the earthquake hypocenter estimation. To illustrate this, the event previously shown in Fig. 1 is used as an example. We performed the localization of this event with the different corrections outlined in the previous sections (Fig. 8).

No correction. By not considering any local corrections, the wave splitting caused by the sediments is not taken into account. In this scenario, the first arrival, hence Pp, is considered as the classical P arrival; the Ps arrival is unmodeled hence discarded; and the Ss arrival is considered as the classical S arrival. In the case presented here (Fig. 8a), the theoretical P-wave moveout matches well with the picked Pp arrivals (which is smooth by nature) while the theoretical S-wave moveout roughly fits the Ss arrivals (which is highly distorted) explaining the overall poor loss. Because the Ss arrival is more delayed by the sediments than the Pp arrival (by approximately the previously defined Δt amount), a location bias is introduced. This extra delay artificially increases the observed time difference between the P and S arrival hence place the hypocenter several kilometers farther from the DAS cable.

As a result of the near-rectilinear geometry of the DAS cable, the localization uncertainty follows a toroidal shape with the cable being the axis of revolution. Consequently, the hypocenter location is well-resolved along the axial and radial directions (i.e., along the North-South cable trajectory and in terms of hypocenter

distance), but is poorly-resolved in term of rotation around the cable axis. The best estimate is positioned at the Earth's surface (Fig. 8m), which is very unlikely to represent the true hypocenter location.

Delay corrections. This correction consists in assuming that the Pp arrival can be considered as the theoretical P arrival while The Ps and Ss arrivals are modeled by adding the Δt delay to the theoretical P and S arrivals. The localization solution, while still exhibiting a toroidal uncertainty profile, presents a more pronounced preferred direction (Fig. 8n). Yet some noticeable mismatch can be observed, particularly for the Ss phase beyond 80 km distance (Fig 8b).

Station corrections. Applying those corrections resulted in the smallest loss, as the model and observations fit almost perfectly (Fig 8c). This is expected. However, as this approach entails inverting 3 parameters per channel, this massive increase in the number of degrees of freedom leads to a reduction of the variance, but likely resulted in overfitting on the data.

Sediment corrections. This approach strikes a balance between simplicity of the parametrization and concordance of the observations with the modeling. With a minimal increase in the loss compared to the station corrections, this approach performs the inversion of only two correction-related parameters in addition to the seismic source parameters. Nevertheless, results are very similar to those obtained with station corrections in terms of the residuals and hypocenter location estimates (Fig. 8d, h, l and p).
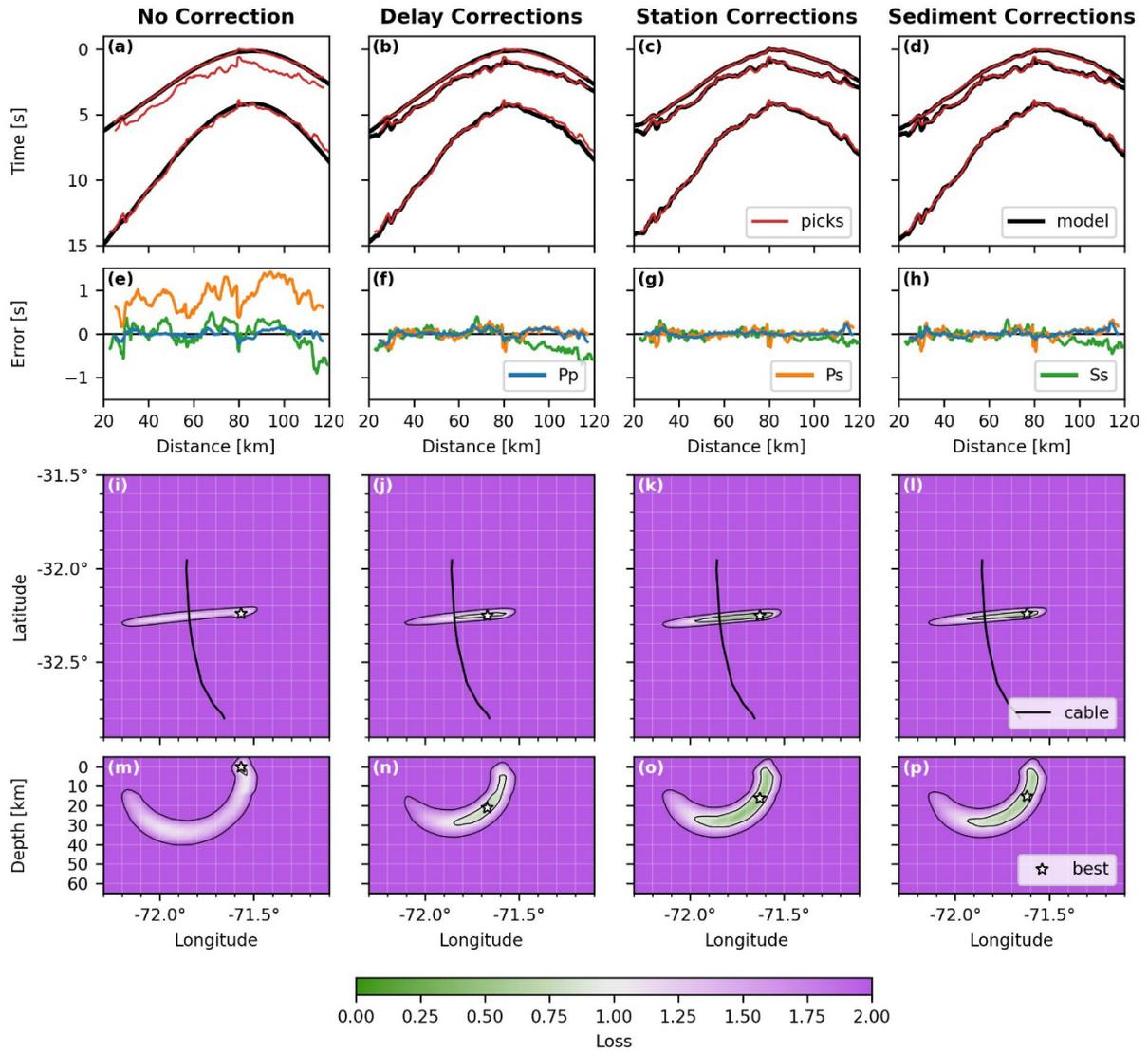
Figure 8. Data adjustment and localization of the event of Fig. 2 using different types of corrections. Each column corresponds to a correction type. (a-d) Observed (red lines, constant from one column to another) and modeled (black lines) arrival times. Time on the vertical axis is given relative to the first pick. Note that for the *no correction* case only a P- and S-wave arrival are modeled. (e-h) Error between observed and modeled arrival times. For the *no correction* case the Ps error is shown but is not considered in the localization procedure. Localization loss: (i-l) on the horizontal plane, and (m-p) on the vertical plane (projections are obtained by keeping minimum values along dimensions). Contours are plotted for loss values of 1.0 and 2.0 along with the optimum location (white star). Note that a larger contoured area does not imply larger uncertainties, as the absolute loss value of the global optimum varies from one panel to the next.

The localization process was then performed for the 30 manually picked earthquakes (Fig. 9). The ambiguity of the localization is manifested by prominent variations of the inferred hypocenter depending on the used correction approach. Yet an overall pattern can be observed. The hypocenters inferred without any form of correction are spread out seemingly randomly, whereas the hypocenters inferred with some forms of correction (delay, station or sediment) are globally located closer to the slab interface. This indicates that the corrections reduce the ambiguity due to the geometry of the cable. The relative performance of the three corrections method is difficult to assess without ground truth.
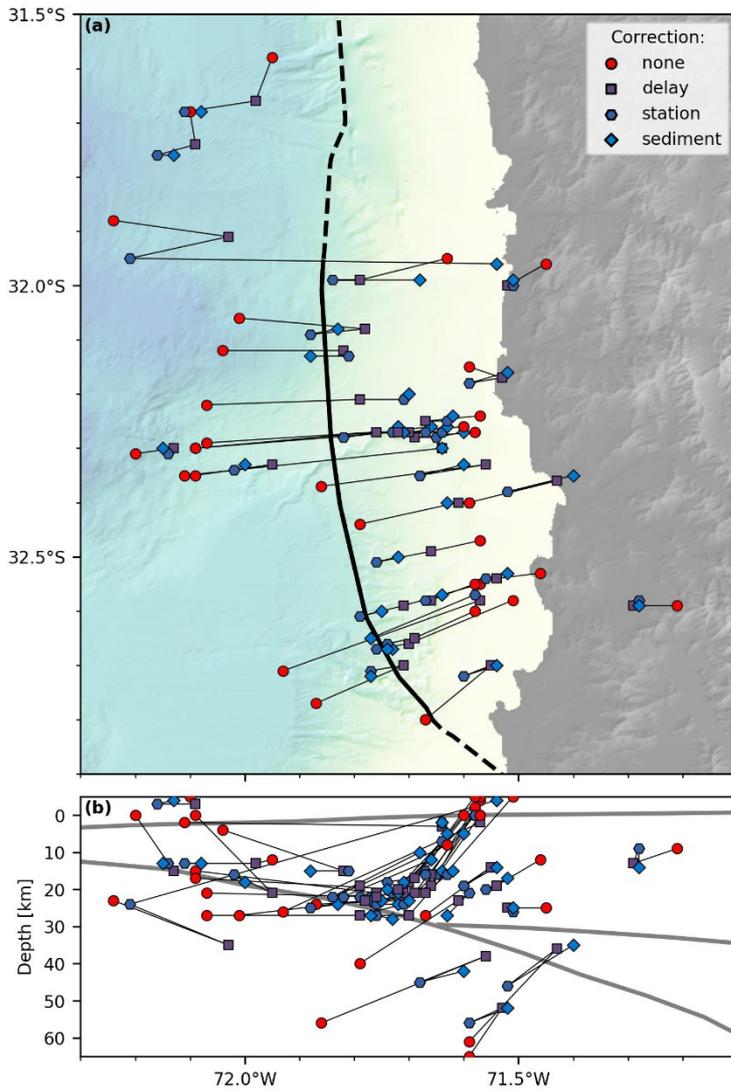
Figure 9. Locations with the different correction methods (plotted as markers of different shape and color) of the 30 events used in that study. (a) Geographic map of the hypocenters. The cable is indicated by the black thick line. (b) Longitude-depth section. The ambiguity due to the almost linear geometry of the cable hinders robust localization. Nevertheless, hypocenters inferred without any corrections look quite spread out whereas corrected hypocenters are attracted along the slab interface direction (gray thick lines are averaged topography, Moho and slab boundaries).

4. Discussion

Considering that the sedimentary layer imposes significant controls on the observed phase arrivals, applying some form of correction is a mandatory step to correctly handle the phase splitting produced by the sediments. The three types of corrections investigated here allow for an improved data adjustment in the localization procedure, reducing the observed to predicted time residuals within the observational uncertainty. The main characteristics of each correction are summarized in Table 1.

The *delay corrections* approach is the most conservative, as it does not require any inversion and is based on the observation of the Pp to Ps delay. It is an easy to implement approach that may be particularly suited for small-scale or short-period deployments where the length of the sensed cable or the number of events is insufficient to perform any significant inversion without overfitting.

Both *station* and *sediment corrections* further increase the data adjustment. The advantage of *sediment corrections* lies in its small number of free parameters and the physical underpinning of the nature of wave propagation

in sediments. This approach requires less data to be properly determined without overfitting and corrections terms are connected to the retrieved physical properties of the sediments. *Sediments corrections* correctly constrain the origin times of the seismic events. This is not the case for *station corrections*, of which the parameters can only be determined up to an arbitrary constant that trades-off with the origin times. Nonetheless, the correction terms that are determined using the *station correction* approach match well with those obtained from the *sediment correction* approach (compare Fig. 5a with Fig. 6a). This indicates that most of the local effects can be attributed to the sedimentary layer.

Table 1. Summary of the different approaches in term of loss, number of measured/inverted parameters (where N is the number of receivers), whether the absolute origin times can be estimated or only up to an unconstrained constant, and whether some valuable physical quantities are retrieved on the sediments structure.

Correction type	Loss	Measured parameters	Inverted parameters	Estimated origin times	Estimation of sediments properties
None	1.75	0	0	Poor	No
Delay	0.74	N	0	Approx.	Limited
Station	0.39	0	3N	No	Indirect
Sediment	0.51	N	2	Yes	Yes

Carefully looking at the residual of the sediment corrections method (that is defined as the mismatch of the applied and required corrections in Fig. 6a) some small large-scale discrepancies can be individuated. Several interpretations of this can be proposed: (i) The positioning of the cable is not known to a sufficient degree of accuracy and introduces some bias in the forward modeling of travel-times. (ii) The nature of the sediments vary along the cable. This argument is particularly pertinent for long or multi-cable deployments covering vast areas. (iii) The properties of the bedrock vary over large scales.

It would be valuable to integrate other external observations to better constrain the problem: (i) seismic shots to relocate the cable and (ii) image the shallow structures of the sediments, (iii) ambient noise or coda wave interferometry to get a prior knowledge on the deeper sediment structure, and (iv) ocean-bottom or on-land stations seismometers to resolve the location ambiguity. Those observations could be joint together with those proposed in this study to make a well-constrained multimodal imagery of the sediments and potentially gain access to local variations of the bedrock properties. Also, the development of detectors capable of natively obtained labelled Pp, Ps and Ss arrivals would allow to enrich the dataset used in the inversions, and to reduce potential overfitting.

5. Conclusions

By carefully analyzing the multiple phase arrivals recorded by a submarine DAS cable, we showed that the arrival time difference between the (direct) Pp to (converted) Ps phases is constant (within the picking uncertainties) at each location along 100-km of an offshore cable. These *delay corrections* can be used to account for the shallow sedimentary layer that causes phase splitting and wavefront distortion. By including these empirical corrections in the hypocenter localization scheme, we significantly reduced the localization residuals. Moreover, to further reduce the impact of local sediments effects, we employed and compared two additional approaches. First, classical *station correction* terms were estimated, which is a conventional approach to capture receiver-specific variations of the phase arrival times. Second, we propose a new approach, termed *sediment corrections*. This later approach builds upon a simple physical model of wave propagation in a distinct sedimentary layer, parameterized by phase velocities and the local sediment thickness (this later being constrained by the averaged measured Pp to Ps delay). As a result, the number of unconstrained parameters reduces from three per channel for *station corrections* to two global parameters (the P- and S-wave velocities in the sediments) for *sediment corrections*. Both approaches yielded similar results

in terms of the variance reduction, and in terms of the spatial variation of the correction terms. This suggests that the shallow sedimentary layer is the main source of local deviations from the global (1D) velocity model. The *station corrections* method is considered to be a simple way of accounting for sediments for localization purposes and is already implemented in many localization codes. However, corrections are determined to within one constant that must be fixed to estimate the origin times; and the large number of unconstrained parameters makes it susceptible to overfitting. In addition to the correction terms that reduce bias in the hypocenter localization, *sediment corrections* give a first global impression of the sediment physical properties which can be used as a validation of the inversion by comparison with typical sedimentary compositions found in the literature.

Acknowledgment

Open Research

To analyze DAS data, the Xdas python package was used (https://github.com/xdas-dev/xdas – https://zenodo.org/doi/10.5281/zenodo.7573823). To perform the manual picking of the DAS data the Xpick toolbox was used (https://github.com/xdas-dev/xpick – https://doi.org/10.5281/zenodo.10678342) . Manual picks and the example of earthquake recordings can be found online (https://doi.org/10.5281/zenodo.10732130). The bathymetry/topography was downloaded using the GMRT MapTool (https://www.gmrt.org/GMRTMapTool). Codes used in this study to analyze data and generate the plots can be found online (https://zenodo.org/records/10782427).

References

Contreras-Reyes, E., Becerra, J., Kopp, H., Reichert, C., & Díaz-Naveas, J. (2014). Seismic structure of the north-central Chilean convergent margin: Subduction erosion of a paleomagmatic arc. *Geophysical Research Letters*, *41*(5), 1523–1529. https://doi.org/10.1002/2013GL058729

Contreras-Reyes, E., Ruiz, J. A., Becerra, J., Kopp, H., Reichert, C., Maksymowicz, A., & Arriagada, C. (2015). Structure and tectonics of the central Chilean margin (31°–33°S): Implications for subduction erosion and shallow crustal seismicity. *Geophysical Journal International*, *203*(2), 776–791. https://doi.org/10.1093/gji/ggv309

Doran, A. K., & Laske, G. (2019). Seismic Structure of Marine Sediments and Upper Oceanic Crust Surrounding Hawaii. *Journal of Geophysical Research: Solid Earth*, *124*(2), 2038–2056. https://doi.org/10.1029/2018JB016548

Douglas, A. (1967). Joint Epicentre Determination. *Nature*, *215*(5096), 47–48. https://doi.org/10.1038/215047a0

Frohlich, C. (1979). An efficient method for joint hypocenter determination for large groups of earthquakes. *Computers & Geosciences*, *5*(3–4), 387–389. https://doi.org/10.1016/0098-3004(79)90034-7

Hamilton, E. L. (1979). $V p / V s$ and Poisson's ratios in marine sediments and rocks. *The Journal of the Acoustical Society of America*, *66*(4), 1093–1101. https://doi.org/10.1121/1.383344

Jeffreys, H., & Singh, K. (1973). Comparison of Station Errors in Seismology. *Geophysical Journal International*, *32*(4), 423–437. https://doi.org/10.1111/j.1365-246X.1973.tb05842.x

Marot, M., Monfret, T., Gerbault, M., Nolet, G., Ranalli, G., & Pardo, M. (2014). Flat versus normal subduction zones: A comparison based on 3-D regional traveltime tomography and petrological modelling of central Chile and western Argentina (29°–35°S). *Geophysical Journal International*, *199*(3), 1633–1654. https://doi.org/10.1093/gji/ggu355

Noble, M., Gesret, A., & Belayouni, N. (2014). Accurate 3-D finite difference computation of traveltimes in strongly heterogeneous media. *Geophysical Journal International*, *199*(3), 1572–1585. https://doi.org/10.1093/gji/ggu358

Pujol, J. (2000). Joint Event Location—The JHD Technique and Applications to Data from Local Seismic Networks. In C. H. Thurber & N. Rabinowitz (Eds.), *Advances in Seismic Event Location* (Vol. 18, pp. 163–204). Springer Netherlands. https://doi.org/10.1007/978-94-015-9536-0_7

Richards-Dinger, K. B., & Shearer, P. M. (2000). Earthquake locations in southern California obtained using source-specific station terms. *Journal of Geophysical Research: Solid Earth*, *105*(B5), 10939–10960. https://doi.org/10.1029/2000JB900014

Trabattoni, A., Biagioli, F., Strumia, C., van den Ende, M., Scotto di Uccio, F., Festa, G., Rivet, D., Sladen, A., Ampuero, J. P., Métaxian, J.-P., & Stutzmann, É. (2023). From strain to displacement: Using deformation to enhance distributed acoustic sensing applications. *Geophysical Journal International*, *235*(3), 2372–2384. https://doi.org/10.1093/gji/ggad365

Trabattoni, A., Festa, G., Longo, R., Bernard, P., Plantier, G., Zollo, A., & Strollo, A. (2022). Microseismicity Monitoring and Site Characterization With Distributed Acoustic Sensing (DAS): The Case of the Irpinia Fault System (Southern Italy). *Journal of Geophysical Research: Solid Earth*, *127*(9). https://doi.org/10.1029/2022JB024529

van den Ende, M. P. A., & Ampuero, J.-P. (2021). Evaluating seismic beamforming capabilities of distributed acoustic sensing arrays. *Solid Earth*, *12*(4), 915–934. https://doi.org/10.5194/se-12-915-2021

Wales, D. J., & Doye, J. P. K. (1997). Global Optimization by Basin-Hopping and the Lowest Energy Structures of Lennard-Jones Clusters Containing up to 110 Atoms. *The Journal of Physical Chemistry A*, *101*(28), 5111–5116. https://doi.org/10.1021/jp970984n

Zhu, J., Canales, J. P., Han, S., Carbotte, S. M., Arnulf, A., & Nedimović, M. R. (2020). Vp/Vs Ratio of Incoming Sediments Off Cascadia Subduction Zone From Analysis of Controlled-Source Multicomponent OBS Records. *Journal of Geophysical Research: Solid Earth*, *125*(6), e2019JB019239. https://doi.org/10.1029/2019JB019239